Effect of bottom stress formulation and tidal forcing on modeled flow and sediment trapping in cross-sections of tide-dominated estuaries

G.P. SCHRAMKOWSKI[1], K.M.H. HUIJTS[2], H.M. SCHUTTELAARS[3] and H.E. DE SWART[2],

1. Flanders Hydraulics, Berchemlei 115, B 2140, Antwerp, Belgium
   email: George.Schramkowski@mow.vlaanderen.be

2. Institute for Marine and Atmospheric research Utrecht, University of Utrecht, PO Box 80000, Utrecht, The Netherlands
   email: h.e.deswart@phys.uu.nl and k.m.h.huijts@phys.uu.nl

3. Delft Institute of Applied Mathematics, Delft University of Technology, Mekelweg 4, 2624 CD, Delft, the Netherlands
   email: h.m.schuttelaars@ewi.tudelft.nl

Keywords: tidal flow, density-driven flow, sediment trapping, tidal rectification

Introduction

Field data collected in cross-sections of tide-dominated estuaries reveal that flow and suspended sediment concentration show pronounced spatial and temporal behavior, which depend on factors like tidal discharge, density gradients and the geometry of the cross-section. Models are capable of reproducing and explaining many aspects of the observations, but also marked discrepancies occur between model results and data. The objective of the present study is to systematically investigate the sensitivity of model output to formulations of physical processes. This is done by comparing two types of models. The first is a numerical model (NM) that solves the full shallow water equations with prognostic salt dynamics. The second is an IM that solves a reduced set of equations for tidal water motion and uses a diagnostic salinity field. The IM can be used as a tool to interpret the complex output of the NM. The NM, on the other hand, can be used to probe the limits of applicability of the IM and may give hints on further improvements of the IM.

Models

The IM results in a 2DV description of the residual and tidal flow in a cross-section of a weakly non–linear, tidally dominated channel without vertical density stratification. The model uses a diagnostic density field and a rigid lid approximation. The cross-sectional bottom profile is Gaussian, with depth $H = H_{\max}$ at the centerline of the channel and $H = 2$ m near the banks, the cross–sectionally averaged water depth is denoted by $\overline{H}$. The barotropic forcing is prescribed by specifying a cross–sectionally averaged M_2 tidal velocity amplitude U. The baroclinic flow results from prescribed residual and M_2 components of the horizontal density gradient. The water surface is stress-free and the velocity vanishes at the bed (no slip). The coefficient of vertical viscosity (A_v) and mixing (K_v) are taken constant and are related to the tidal flow U and average bottom depth by the relation

$$A_v = K_v = 0.002 U \overline{H}. \tag{1}$$

The NM solves the three–dimensional shallow water equations with a prognostic density field and a free lid. To be able to compare the numerical model results with those obtained with the IM, the setup of the NM is chosen such that it mimics the basic assumptions of the IM as close as possible. Therefore, the model geometry describes a tidal channel of length 1200 km and uniform width B=5 km. At the seaward entrance of the channel, an M_2 water level forcing (circular frequency σ) is imposed. The landward entrance is an open boundary on which zero discharge is prescribed. At a distance of 400 km from the seaward entrance, the cross-section is identical to the Gaussian bed profile in the IM. Only results in this cross–section are compared to the idealised model results. For further details, see Schramkowski et al. (2007).

For the NM a density difference between the seaward and landward entrance is imposed such that the residual along–channel density gradient of the NM equals the gradient imposed in the IM which is $\sim 10^{-4} \mathrm{kg\,m^{-4}}$. To get similar forcings in both models, the following procedure is performed: first, a value for U is chosen. To get this value in the NM runs, the tidal boundary conditions are varied such that the required U is obtained at

the cross–section. Finally, the residual and semi–diurnal parts of the depth–averaged density gradients, that are self–consistently calculated with the NM, are adopted as baroclinic forcing to the IM.

Finally, the hydrodynamics results from both NM and IM are used to solve the residual SSC from a sediment transport module (STM) a posteriori. This STM uses a morphodynamic equilibrium condition, which implies that the net lateral sediment flux (advective plus diffusive) vanishes. For a detailed discussion, see Huijts et al. (2006).

Methods

To assess the applicability of the IM, the IM results are compared with those obtained by the NM. To do this in an objective manner, we compare the residual and M_2 parts of velocity components (u, v, w) and sediment concentration c. Here u, v and w refer to along–channel, lateral and vertical velocity. Tidal components will be denoted by subscripts (e.g. u_{M0}). A good agreement is defined by a correlation coefficient larger than 0.75 and the ratio of the largest values between 0.3 and 3.

Results

For the IM and the NM, several experiments have been performed for a range of tidal flow velocities $(0.1 < U < 1 \text{ m s}^{-1})$ and maximum bottom depth values $(H_{\max} = 10, 15, 30 \text{ and } 60 \text{ m})$. The results are summarised in sensitivity diagrams, i.e. plots that show the variation of a quantity with U and $H_{\max}$. Figure 1 shows three diagrams that give information about the applicability of the IM by probing the validity of its basic assumptions. First, Fig. 1a gives maximum vertical difference in residual density. If this becomes too large,
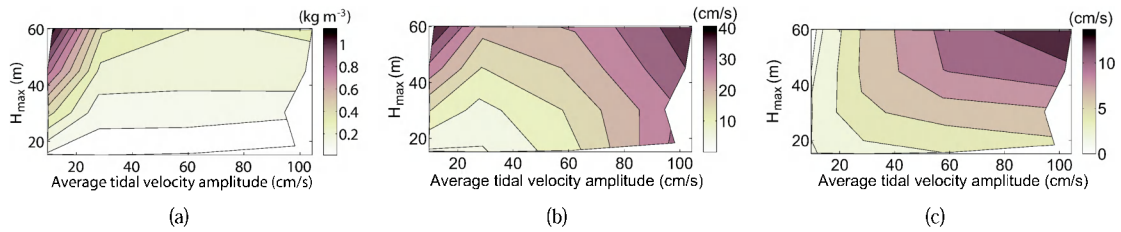

Figure 1: Several sensitivity diagrams: (a) maximum bed minus surface residual density difference, (b) maximum along-channel residual flow and (c) maximum across-channel tidal flow.

the assumption of weak vertical stratification is violated. This occurs for situations with low tidal velocity U and large water depth. Figure 1b gives the along-channel residual velocity. If this becomes comparable to the along-channel directed tidal flow, the flow is no longer tidally dominated. Finally, the IM assumes that the flow is weakly non-linear, i.e. that advective terms in the momentum equations are small. This is not justified if the cross-channel tidal excursion length becomes comparable to the channel width B, i.e. if the lateral tidal velocity v_{M2} becomes too large. This occurs for high tidal velocity U and large depths (see Fig 1c).

Nonetheless the actual applicability of the IM turns out to depend on the physical quantity and harmonic constituent under consideration. Explicitly, we found that:

- u_{M2} is well represented in all considered parameter ranges

- v_{M2} is not well computed for low tidal flow and large depths.

- u_{M0} is not correctly modellel for large tidal flow and large water depth

- v_{M0} is not calculated accurately for low tidal flow and fairly large water depth

Hence, if the main interest is in the trapping of sediment, the IM is applicable for all parameter values except for small tidal velocities and large water depth. This is because the lateral sediment transport is governed by the residual v_{M0} and tidal u_{M2} (see Huijts et al. 2006). This is confirmed by the sensitivity diagram in 2a. The resulting SSC also shows good agreement between IM and NM in the same parameter regime, with the SSC mainly found at the left bank. Figure 2b shows this distribution for the case where $U = 0.6 \text{ ms}^{-1}$ and $H_{\max} = 30 \text{ m}$, which is within the region where IM and NM agree.
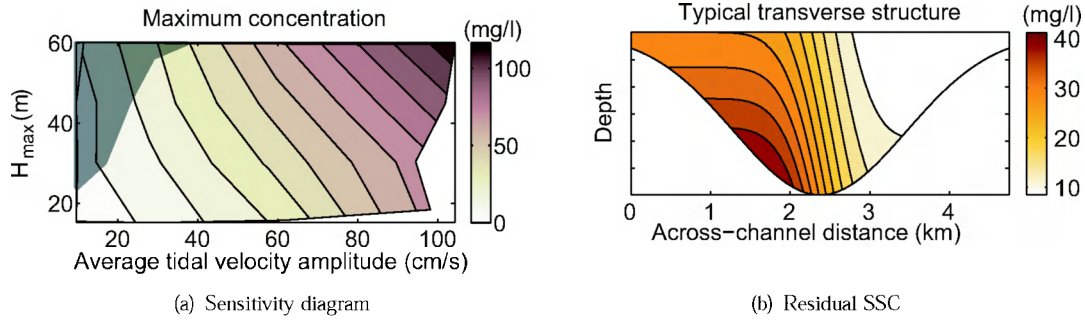
(a) Sensitivity diagram

(b) Residual SSC

Figure 2: Left: sensitivity diagram for the residal SSC. The dark region indicates where the IM is not valid. Right: cross-sectional distribution of the residual SSC for $U = 0.6\,\mathrm{ms}^{-1}$ and $H_{\mathrm{max}} = 30\,\mathrm{m}$.

Finally, for the same parameter settings, Fig. 3 shows the NM and IM results for the residual part of the along-channel velocity component. It is clear that the results are in good qualitative and quantitative agreement.
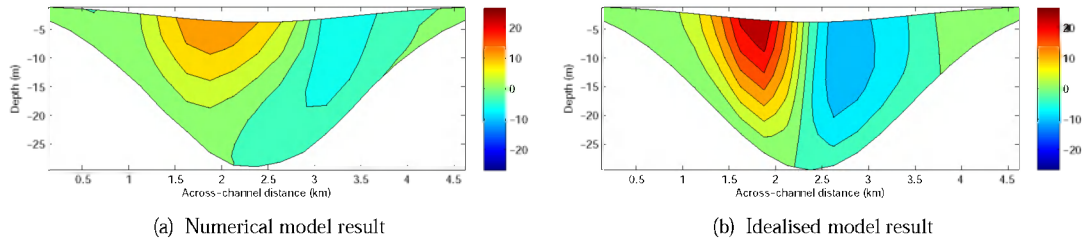

(a) Numerical model result

(b) Idealised model result

Figure 3: Residual along-channel velocity for $U = 0.6\,\mathrm{ms}^{-1}$ and $H_{\mathrm{max}} = 30\,\mathrm{m}$. Left: numerical model, right: idealised model. The velocity scale is in $\mathrm{cm\,s}^{-1}$.

Discussion

By combining the results of the IM and the NM, we have been able to use the NM to examine the validity of the IM (see Fig. 1). Conversely, we can use the IM to interpret NM results for parameter settings where both models give similar results. As an example, we will elaborate on the result for the residual along-channel flow that is shown in Fig. 3. Using the IM, is it possible to identify four major mechanisms that can contribute to the
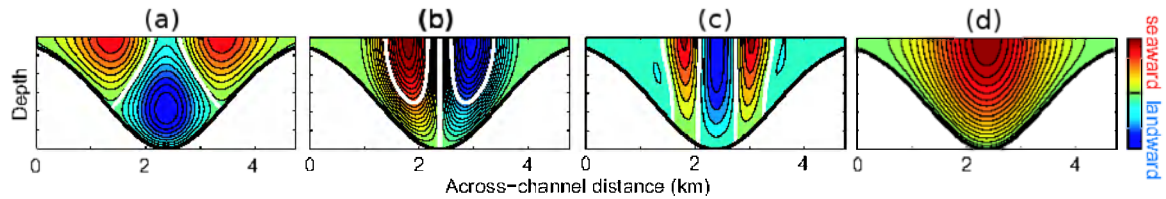

Figure 4: Four major mechanisms that contribute to the along-channel residual flow. Red (blue) is seaward (landward) directed flow.

residual along-channel flow (see Fig. 4). The first is the classical gravitational circulation (Fig. 4a), which has relatively light (heavy) water moving seaward (landward) in the upper (lower) parts of the water column. This flow pattern is expected to be prominent at low tidal flow velocities. Figure 4b shows a horizontally stratified flow with inflow (outflow) located on the right (left) part of the cross-section. This contributing is due to tidal rectification by the Coriolis force. It arises from advection of the along-channel directed M_2 flow u_{M_2} by the Coriolis induced cross-channel M_2 circulation (v_{M_2}, w_{M_2}) (Huijts et al. 2007). This cross-channel circulation consist of a single gyre (not shown). Figure 4c also stems from rectification, but here the main along-channel

tide is advected with semi-diurnal cross-channel circulation that stems from the M_2 component of the lateral density gradient. This lateral circulation consist of double gyre pattern (not shown) which reflects the fact the M_2 density variation has a larger amplitude in deeper parts. Finally, Fig. 4d shows the residual flow that is related to the Stokes return flow. This flow is not included in the IM since it uses a rigid lid approximation. However, the NM does include free surface effects, so that it is possible to compute the discharge associated with the Stokes return flow. This discharge is then imposed in the IM.

It is clear from the results in Fig. 4 that the Coriolis induced tidal rectification effect is the dominant mechanism in the situation shown in Fig. 3. Hence we see that the IM can be used as a means to identify key physical mechanisms in a NM result.

Conclusions and outlook

From the results presented above we conclude the following:

- the NM can be used to test validity of the IM, but the eventual reliability of the IM depends on the physical quantity and the tidal component of interest. In this respect, the IM may be more widely applicable than indicated by the sensitivity diagrams (Fig. 1).

- the IM is able to describe lateral sediment trapping adequately, provided that the tidal flow is not too low or the water depth not too large (Fig. 2).

- the IM can be used as a tool to interpret the outcome of the NM when both give similar results.

Recently, we have been extending the study by incorporating a partial slip formulation for the bed shear stress. This is motivated by the fact that it is inconsistent to use a no slip condition in conjunction with a constant vertical viscosity. As an alternative, one may put the near-bed boundary physically at the top of the constant stress layer rather than at the true bed. At this interface, it then realistic to adopt a partial slip condition.

It appears that the use of partial slip instead of no slip may have considerable consequences. As an example, let us consider the residual along-channel velocity u_{M0} once more. For partial slip, the relative importance of Coriolis driven tidal rectification (Fig. 4b) will decrease. Indeed, the Coriolis driven lateral circulation is essentially driven by the vertical shear in the along-channel tidal flow. If one allows for velocity slip at the bed, the along-channel velocity will show less vertical variation, which indicates that the Coriolis driven lateral tidal flow will be smaller compared to the case where no slip is used. Hence we expect the Coriolis related tidal rectification to be a less important contributor to u_{M0}. The baroclinic contribution to u_{M0} (Fig. 4c), however, will not decrease since the vertical variation of baroclinic forcing is less sensitive to velocity slip. Hence, we expect a relatively larger contribution from this mechanism if velocity slip is introduced.

By the same line of reasoning, we expect the IM to be more applicable if a partial slip formulation is used. Since velocity slip will lead to a decrease of the Coriolis induced lateral tidal circulation, it will give a lower value of $v_{M2}/(\sigma B)$. As a consequence, we expect the assumption of weak non-linearity that underlies the IM (see Fig. 1c) to be valid over a larger range of the parameters U and $H_{\max}$.

References

Huijts, K.M.H., Schuttelaars, H.M., de Swart, H.E., Valle-Levinson, A. (2006), Lateral trapping of sediment in tidal estuaries: an idealized model, *J. Geophys. Res.*, 111, C12016, doi:10.1029/2006JC003615

Huijts, K.M.H., Schuttelaars, H.M., de Swart, H.E., Friedrichs, C.T. (2007), Analytical study of the transverse distribution of along-channel and transverse residual flows in tidal estuaries, *Cont. Shelf Res.*, doi:10.1016/j.csr.2007.09.007

Schramkowski, G.P., Huijts, K.M.H., Schuttelaars, H.M., de Swart, H.E. (2007), A model comparison of flow and lateral sediment trapping in estuaries, in *River, Coastal and Estuarine Morphodynamics: RCEM 2007, C.M. Dohmen-Janssen & S.J.M.H. Hulscher (eds)*, 413–420